PCCP

PAPER

View Article Online
View Journal | View Issue

Cite this: *Phys. Chem. Chem. Phys.*, 2021, **23**, 24750

Aromaticity reversals and their effect on bonding in the low-lying electronic states of cyclooctatetraene†

Peter B. Karadakov * and Nicholas Preston

Received 24th September 2021,
Accepted 21st October 2021

DOI: 10.1039/d1cp04394c

rsc.li/pccp

Aromaticity reversals and their effect on chemical bonding in the low-lying electronic states of cyclooctatetraene (COT) are investigated through a visual approach which examines the variations in isotropic magnetic shielding in the space surrounding the molecule. The ground state (S_0) of COT is shown to be strongly antiaromatic at the π-bond-shifting transition state (TS), a regular octagon of D_{8h} symmetry; S_0 antiaromaticity decreases at the D_{4h} planar bond-alternating tub-to-tub ring-inversion TS but traces of it are shown to persist even at the tub-shaped D_{2d} local minimum geometry. The lowest triplet (T_1) and first singlet excited (S_1) states of COT are found to have very similar D_{8h} geometries and visually indistinguishable shielding distributions closely resembling that in benzene and indicating similarly high levels of aromaticity. Unexpectedly, COT diverges from its antiaromatic predecessor, cyclobutadiene, in the properties of the second singlet excited state (S_2): In cyclobutadiene S_2 is antiaromatic but in COT this state turns out to be strongly aromatic, with a shielding distribution closely following that around S_2 benzene.

Introduction

Cyclooctatetraene (C_8H_8, COT) has been aptly described as "one of the decisive molecules in the history of chemistry".[1] It has been the subject of numerous experimental and theoretical studies; a comprehensive account of pre-2012 research has been provided by Schleyer and co-workers.[1] The ground-state (S_0) potential energy surface (PES) of COT has been examined in considerable detail[2–8] and has been found to include symmetry-equivalent tub-shaped local minima of D_{2d} symmetry connected through planar tub-to-tub ring-inversion transition states (TS) of D_{4h} symmetry; these, in turn, are connected through a planar π-bond-shifting TS in the form of a regular octagon of D_{8h} symmetry. In its electronic ground state D_{8h} COT is a singlet diradical and its full-symmetry description requires at least a two-determinant wavefunction; the attempt to use the standard single closed-shell Slater determinant results in a "broken-symmetry" wavefunction which suggests energetically favourable distortions of the nuclear framework to one of the two bond-alternating D_{4h} geometries. As shown by Hrovat and Borden,[3] the ground-state PES of COT can be described with high accuracy using a complete active-space self-consistent field (CASSCF) wavefunction with "8 electrons in 8 orbitals", CASSCF(8,8), accounting for the eight electrons involved in the bond rearrangements linking the D_{2d}, D_{4h} and D_{8h} stationary points; CASSCF(8,8) wavefunctions have been also found to work well in studies of several low-lying electronic states of COT.[4,6,9,10]

Hückel molecular orbital (HMO) theory depicts the ground electronic state of D_{8h} COT as an antiaromatic triplet which is incorrect in more than one way: Firstly, at this geometry COT has an antiaromatic singlet ground electronic state which violates Hund's rule and secondly, the lowest triplet state (T_1) of D_{8h} COT has been shown to be aromatic.[10–13] D_{8h} COT was used by Baird as an example of a molecule featuring an aromaticity reversal on excitation from S_0 to T_1;[11] subsequent research revealed that D_{8h} COT experiences a similar aromaticity reversal on excitation from S_0 to the first singlet excited state (S_1).[10] Recent experimental work has demonstrated that cyclooctatetraene-fused acene dimers exhibit remarkable conformational flexibility associated with the change in aromaticity of the central COT moiety on excitation from S_0 to S_1; such "flapping" fluorophores (FLAP) provide a versatile platform for designing novel photofunctional systems.[14–16]

Department of Chemistry, University of York, Heslington, York, YO10 5DD, UK. E-mail: peter.karadakov@york.ac.uk

† Electronic supplementary information (ESI) available: Isotropic shielding contour plots for the S_0 (at D_{4h} and D_{8h} geometries), T_1, S_1 and S_2 (at D_{8h} geometries) electronic states of COT in planes 1 Å above the respective molecular planes and in planes perpendicular to the molecular planes; computational details and D_{2d} S_0 and D_{4h} S_0 optimised geometries; details of the compositions of the CASSCF wavefunctions for the S_0, S_1, S_2 and T_1 electronic states of D_{8h} COT (PDF). Zip archive of Gaussian cube files with isotropic shielding values for the S_0 (at D_{2d}, D_{4h} and D_{8h} geometries), T_1, S_1 and S_2 (at D_{8h} geometries) electronic states of COT (ZIP). See DOI: 10.1039/d1cp04394c

In this paper we investigate aromaticity and chemical bonding at all stationary points of the ground-state PES of COT, including the D_{2d} tub-shaped, D_{4h} bond-alternating and D_{8h} geometries, as well as at the D_{8h} geometries of the lowest triplet and first and second singlet (T_1, S_1 and S_2) electronic excited states by analysing, for each geometry and electronic state, the changes in the off-nucleus isotropic shielding, $\sigma_{iso}(\mathbf{r}) = 1/3[\sigma_{xx}(\mathbf{r}) + \sigma_{yy}(\mathbf{r}) + \sigma_{zz}(\mathbf{r})]$, within the space surrounding the molecule. All $\sigma_{iso}(\mathbf{r})$ calculations make use of state-specific CASSCF(8,8) wavefunctions constructed from gauge-including atomic orbitals (GIAOs). The aromaticities of the S_0, T_1 and S_1 states of COT have been examined at the CASSCF(8,8)-GIAO level[10] with several types of nucleus-independent chemical shifts (NICS),[17–22] proton shieldings and magnetic susceptibilities. However, when applying NICS in order to assess the aromaticity of a larger ring such as COT, it is logical to ask to what extent we can trust predictions based on a single shielding value calculated at or above the centre of this ring. In contrast to NICS and other single-value aromaticity criteria, $\sigma_{iso}(\mathbf{r})$ isosurfaces and contour plots provide somewhat more detailed and, arguably, more reliable information about aromaticity and its effect on chemical bonding.[23–27] Representing off-nucleus magnetic isotropic shielding as a function of position in the space surrounding a molecule requires a very large number of closely spaced data points which addresses potential deficiencies of single-point NICS such as the need to choose, in a more or less arbitrary manner, locations at which these quantities are calculated (NICS can exhibit strong positional dependence and, in certain situations, standard choices can be inappropriate[28,29]), and the argument that a single number might not be sufficient to characterise all aspects of aromatic behaviour, supported by the observation that different ring current maps can produce nearly indistinguishable single-point NICS values.[30,31] The application of this approach to the low-lying electronic states of the archetypal examples of aromatic and antiaromatic systems, benzene (C_6H_6) and square cyclobutadiene (C_4H_4)[24] has shown that the profoundly different shielding distributions in the S_0 states of C_6H_6 and C_4H_4 can be viewed as aromaticity and antiaromaticity "fingerprints" which are reproduced in other electronic states of the two molecules and allow classification of these states as aromatic (S_0 and S_2 for C_6H_6, T_1 and S_1 for C_4H_4) or antiaromatic (S_0 and S_2 for C_4H_4, T_1 and S_1 for C_6H_6); S_2 C_6H_6 was predicted to be even more aromatic than S_0 C_6H_6. Whether or not the low-lying electronic states of D_{8h} COT follow a pattern similar to that observed in its antiaromatic cyclic conjugated predecessor with $4n$ π electrons, square cyclobutadiene, is one of the questions targeted through the research reported in this paper.

Computational procedure

The active spaces in the state-specific CASSCF(8,8) wavefunctions for the S_0, T_1, S_1 and S_2 states of D_{8h} COT studied in this paper were formed from the π-orbital configuration $(a_{2u})^2(e_{1g})^4(e_{2u})^2$ and two higher-energy π orbitals, a doubly-degenerate e_{3g} and a b_{2u}. As explained in ref. 10, the symmetries of the singlet and triplet states associated with the direct product $e_{2u} \times e_{2u}$ follow from the compositions of its symmetric and antisymmetric parts, $[e_{2u} \times e_{2u}] = a_{1g} + b_{1g} + b_{2g}$ and $\{e_{2u} \times e_{2u}\} = a_{2g}$, respectively. Thus $e_{2u} \times e_{2u}$ gives rise to three singlet states, 1^1A_{1g} (S_1), 1^1B_{1g} (S_0) and 1^1B_{2g} (S_2), and one triplet state, 1^3A_{2g} (T_1). The largest subgroup of the D_{8h} point group supported by one of the program packages we used for CASSCF(8,8) calculations, Dalton,[32] is D_{2h}, therefore in that subgroup the S_0, S_1, S_2 and T_1 states of D_{8h} COT were treated as the 1^1B_{1g}, 1^1A_g, 2^1A_g and 1^3B_{1g} states, respectively. The 2^1A_g state was accessed by requesting the second root of the CASSCF(8,8) configuration interaction (CI) problem in that symmetry. In the CASSCF(8,8) calculations carried out with Gaussian16[33] the S_1 and S_2 states were accessed by requesting the second and third roots, respectively, of the CASSCF(8,8) CI problem. The selection of active-space orbitals for the CASSCF(8,8) wavefunctions for the S_0 states of D_{4h} and D_{2d} COT was, in each case, a straightforward task.

The CASSCF(8,8)/6-31G** optimised geometries of the 1^1B_{1g} state of D_{8h} COT (TS for the π bond shift process on the S_0 PES), the 1^1A_{1g} state of D_{4h} COT (TS for the ring inversion process on the S_0 PES), the 1^1A_1 state of D_{2d} COT (local minimum on the S_0 PES), the 1^3A_{2g} state of D_{8h} COT (local minimum on the T_1 PES) and the 1^1A_{1g} state of D_{8h} COT (local minimum on the S_1 PES) were taken from an earlier study of COT.[10] Additionally, the geometry of the 1^1B_{2g} state of D_{8h} COT (local minimum on the S_2 PES) was optimised at the same CASSCF(8,8)/6-31G** level, and then the geometries of all stationary points on the S_0, T_1, S_1 and S_2 PES of COT studied in this paper were reoptimised at the CASSCF(8,8)/cc-pVTZ level. As the differences between the CASSCF(8,8)/6-31G** and CASSCF(8,8)/cc-pVTZ optimised geometries were observed to be minor, all subsequent magnetic shielding calculations were carried out at the CASSCF(8,8)/6-31G** geometries; according to our experience with calculations of this type, off-nucleus shieldings are relatively insensitive to minor changes in molecular geometry. All of the additional geometry optimizations were carried out using Gaussian16[33] and the local minimum or saddle point nature of each optimised geometry was verified through an analytic harmonic frequency calculation.

All CASSCF(8,8)-GIAO calculations were performed by means of the MCSCF-GIAO (multiconfigurational SCF with GIAOs) methodology[34,35] that is implemented in the Dalton program package;[32] the basis set used in these calculations was 6-311+G*. All reported total energies of various electronic states at CASSCF(8,8)/6-31G** geometries were also computed within the 6-311+G* basis, with both Gaussian16 and Dalton. Following previous work on NICS[10,12,24,36] and ring currents[37] in triplet systems, the CASSCF-GIAO isotropic shieldings in the lowest triplet electronic state of COT reported in this paper include only contributions that arise from the perturbation to the wavefunction. With this choice, the values reported for a triplet state can be compared directly with those for singlet states. For comparisons to experimental data when and if such data becomes available, one will need to take into account the large terms associated

with the interaction between the electronic spin angular momentum and the magnetic field.[38,39]

The grids of points used in the construction of $\sigma_{iso}(\mathbf{r})$ isosurfaces and contour plots for the S_0, T_1, S_1 and S_2 electronic states of COT studied in this paper are regular, with a spacing of 0.05 Å, in the shape of rectangular boxes centred at the origins of centre-of-mass right-handed Cartesian coordinate systems in which the z axes are oriented along the respective principal symmetry axes and the x and y axes are oriented along the C_2' axes (D_{2d} geometry) or the C_2'' axes (D_{4h} and D_{8h} geometries). The grid for the S_0 state of D_{2d} COT consists of $133^2 \times 81$ points, and the grids for all other states consist of $161^2 \times 101$ points. In order to reduce computational effort, the $\sigma_{iso}(\mathbf{r})$ values for each electronic state were calculated only at symmetry-unique grid points (1/4 of all points for D_{2d} COT and 1/8 of all points for D_{4h} and D_{8h} COT, respectively) and data were then replicated by symmetry. For visualization purposes, all $\sigma_{iso}(\mathbf{r})$ values obtained for the electronic states of COT were assembled into Gaussian cube files.[40]

Results and discussion

The carbon–carbon and carbon-hydrogen bond lengths in the S_0, T_1, S_1 and S_2 electronic states of COT from geometries optimised using state-specific CASSCF(8,8) wavefunctions in the 6-31G** and cc-pVTZ basis sets are shown in Table 1 together with the lowest harmonic frequencies and total energies of these states. The carbon–carbon and carbon–hydrogen bond lengths calculated in the cc-pVTZ basis set are slightly shorter; the largest difference between 6-31G** and cc-pVTZ bond lengths of 0.0052 Å is observed for the carbon–carbon ''double'' bond in D_{2d} COT.

The results for the electronic states of D_{8h} COT obtained in the cc-pVTZ basis provide further indication that the antiaromatic S_0 and aromatic T_1 and S_1 geometries can be expected to be very similar, with carbon–carbon bond lengths closer to that in benzene and significantly shorter than that in cyclobutadiene, 1.3961 Å and 1.4434 Å, respectively, from CASSCF(6,6)/6-31G** and CASSCF(4,4)/6-31G** S_0 geometry optimizations of D_{6h} benzene and D_{4h} cyclobutadiene.[10] The carbon–carbon bond length in the S_2 D_{8h} COT geometry is almost identical to that in S_0 benzene, with a difference of just 0.0004 Å (in the 6-31G** basis), which suggests an increase in aromaticity in comparison to T_1 and S_1 COT.

The variations in isotropic shielding around the S_0, T_1, S_1 and S_2 electronic states of COT at the CASSCF(8,8)/6-31G** geometries reported in Table 1 are illustrated in Fig. 1. The isovalues of $\sigma_{iso}(\mathbf{r}) = \pm 16$ ppm and the molecular orientations were chosen so as to show reasonable levels of detail. Other orientations and isosurfaces for other isovalues can be examined using the Gaussian cube files with isotropic shielding values for the different geometries and electronic states of COT that are included in the ESI.† Further information about the behaviour of the isotropic shielding in the electronic states of COT at the planar D_{4h} and D_{8h} geometries is provided by contour plots in three planes: the molecular plane (Fig. 2), a plane 1 Å above it, and a plane perpendicular to the molecular plane (Fig. S1 and S2 in the ESI†).

The shielding along the carbon framework in the S_0 electronic ground state at the D_{2d} tub-shaped geometry outlines a sequence of alternating ''single'' and ''double'' carbon–carbon bonds similar to those reported in the magnetic shielding study of bonding in *trans*-1,3-butadiene.[41] It is interesting to observe that this clearly non-aromatic picture retains a minor hint of antiaromaticity in the form of a small deshielded region surrounded by the yellow $\sigma_{iso}(\mathbf{r}) = -1$ ppm isosurface in the centre of the ring. Note that other parts of this isosurface at –1 ppm can be seen as larger ''halos'' over the smaller orange ''halos'' at –16 ppm surrounding carbon atoms familiar from previous magnetic shielding studies of conjugated systems involving sp^2 and sp hybridised carbon atoms and other sp^2 hybridised first main row atoms.[23,24,27,42,43] A recent study of magnetically induced currents in D_{2d} COT reported a weak paratropic global molecular ring current,[8] an indication of a very low level of antiaromaticity, which is in line with the findings of the current work. The shielding along the carbon framework does not show signs of additional conjugation over that in *trans*-1,3-butadiene[41] which suggests that the interesting concept of ''two-way'' (double) hyperconjugation in D_{2d} COT[1] is

Table 1 Carbon–carbon and carbon–hydrogen bond lengths (Å), lowest harmonic frequencies (cm^{-1}) and total energies (E_h) for the S_0, T_1, S_1 and S_2 electronic states of COT from CASSCF(8,8) calculations in the 6-31G**, cc-pVTZ and 6-311 + G* basis sets; ''6-31G**'' rows show CASSCF(8,8)/6-311 + G*//CASSCF(8,8)/6-31G** total energies. S_0, T_1 and S_1 data at CASSCF(8,8)/6-31G** geometries from ref. 10. D_{4h} and D_{8h} S_0 TS geometries; local minimum geometries for all other states

Geometry	State	Basis	R(CC)	R(CH)	υ_1	Energy
D_{2d}	S_0 (1^1A_1)	6-31G**	1.3436, 1.4794	1.0791	179.8 (a_1)	–307.691 721
		cc-pVTZ	1.3384, 1.4767	1.0767	180.5 (a_1)	–307.735 840
D_{4h}	S_0 (1^1A_{1g})	6-31G**	1.3510, 1.4718	1.0777	112.6i (b_{2u})	–307.674 646
		cc-pVTZ	1.3454, 1.4705	1.0753	144.4i (b_{2u})	–307.718 937
D_{8h}	S_0 (1^1B_{1g})	6-31G**	1.4081	1.0774	2304.0i (b_{2g})	–307.663 411
		cc-pVTZ	1.4044	1.0750	2595.3i (b_{2g})	–307.707 176
	T_1 (1^3A_{2g})	6-31G**	1.4063	1.0773	159.5 (e_{2u})	–307.638 857
		cc-pVTZ	1.4026	1.0750	162.4 (e_{2u})	–307.682 884
	S_1 (1^1A_{1g})	6-31G**	1.4074	1.0772	157.7 (e_{2u})	–307.612 618
		cc-pVTZ	1.4036	1.0748	160.1 (e_{2u})	–307.656 593
	S_2 (1^1B_{2g})	6-31G**	1.3957	1.0773	162.8 (e_{2u})	–307.557 953
		cc-pVTZ	1.3927	1.0749	166.0 (e_{2u})	–307.603 528

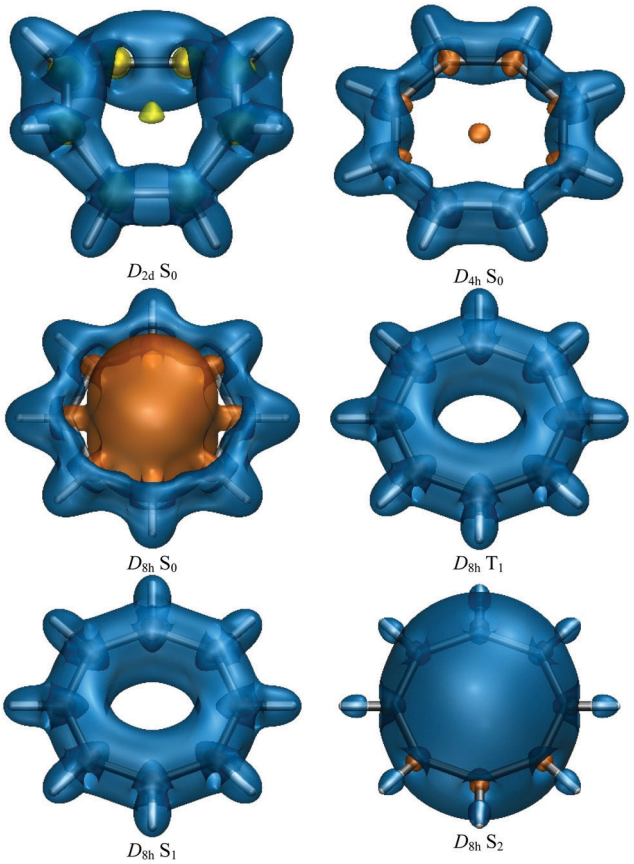

Fig. 1 Isotropic shielding isosurfaces at $\sigma_{iso}(\mathbf{r})$ = ±16 ppm (" +" in blue, "−" in orange) for the electronic states of COT studied in this paper; additional $\sigma_{iso}(\mathbf{r})$ = −1 ppm isosurface (yellow) included for S_0 (D_{2d} geometry). For details, see text.

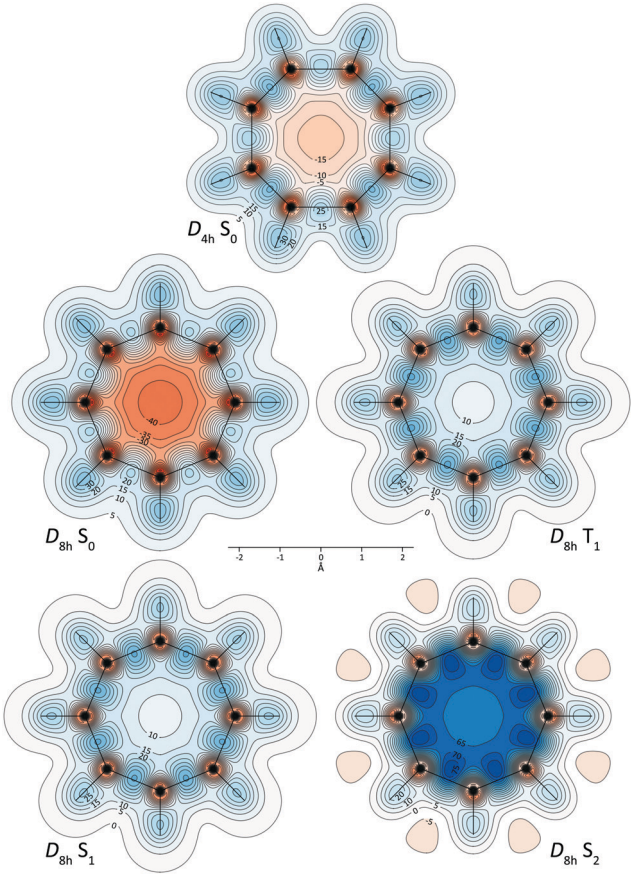

Fig. 2 Isotropic shielding contour plots in the molecular (horizontal) planes for the S_0 state of D_{4h} COT and the S_0, T_1, S_1 and S_2 states of D_{8h} COT. Contour levels at −75(5)75 ppm, orange (deshielded) to blue (shielded).

likely to make only a minor contribution to bonding in this molecule.

The differences between the shielding around "single" and "double" carbon–carbon bonds are still obvious but somewhat less pronounced at the S_0 planar geometry of D_{4h} symmetry. There is some more evidence of antiaromaticity at the ring centre, in the form of a small almost spherical deshielded region with a boundary at –16 ppm. In fact, the D_{4h} S_0 $\sigma_{iso}(\mathbf{r})$ contour plot in Fig. 2 indicates that most of the interior of the carbon ring is moderately deshielded, including a sizeable region deshielded by more than 10 ppm. Antiaromaticity is also manifested by the weakened shielding around carbon–carbon bonds, the bulk of which is displaced away from the ring centre; this affects more the four "single" bonds.

The ground-state antiaromaticity of COT is most pronounced at the D_{8h} planar geometry, at which the shielding picture is dominated by a large strongly deshielded dumbbell-shaped region in the centre of the molecule. The presence of this strongly deshielded region leads to further reduction of the shielding around carbon–carbon bonds and further displacement of this shielding towards the exterior of the ring. The variations in isotropic shielding around S_0 D_{8h} COT resemble closely those observed for the paradigm of antiaromaticity, the electronic ground state of square cyclobutadiene.[24] It has been suggested, on the basis of NICS values, that the S_0 state of D_{8h} COT is more antiaromatic than the respective state of square cyclobutadiene.[10] Indeed, the deshielding of the ring interior shown in Fig. 1, 2 and Fig. S1, S2 (ESI†) is more intensive than that seen in analogous contour plots for square cyclobutadiene[23,24] but, at the same time, in COT the extent to which the central deshielded region disrupts the shielding around carbon–carbon bonds is smaller. It would be correct to say that while the S_0 state of D_{8h} COT is undoubtedly strongly antiaromatic, antiaromaticity affects bonding along the carbon framework to a lesser degree than in the respective state of square cyclobutadiene. This is in line with the similarity between the antiaromatic S_0 and aromatic T_1 and S_1 D_{8h} COT geometries illustrated by the data in Table 1.

Clearly, $\sigma_{iso}(\mathbf{r})$ isosurfaces and contour plots differentiate between the levels of aromaticity of ground-state COT at its D_{8h}, D_{4h} and D_{2d} geometries in a more nuanced way than modern valence bond (VB) theory: According to a spin-coupled generalised valence-bond (SCGVB) study,[44] antiaromaticity at the D_{8h} geometry follows from the singlet biradical character of the wavefunction (triplet pairs coupled to an overall singlet), whereas the absence of resonance within the wavefunctions

Table 2 Carbon and proton isotropic shieldings and NICS values for the S_0, T_1, S_1 and S_2 electronic states of COT. CASSCF(8,8)-GIAO/6-311 + G*//CASSCF(8,8)/6-31G** results, all in ppm

Geometry	State	$\sigma_{iso}(^{13}C)$	$\sigma_{iso}(^{1}H)$	NICS(0)	NICS(1)	$NICS(0)_{zz}$	$NICS(1)_{zz}$
D_{2d}	S_0 (1^1A_1)	76.57	27.26	1.16	−1.57	14.08	4.21
D_{4h}	S_0 (1^1A_{1g})	79.48	28.91	16.10	11.98	55.40	37.62
D_{8h}	S_0 (1^1B_{1g})	70.21	31.70	40.71	32.23	128.71	98.22
	T_1 (1^3A_{2g})	81.93	25.57	−8.93	−8.98	−20.64	−25.60
	S_1 (1^1A_{1g})	80.01	25.43	−8.87	−9.02	−21.52	−26.34
	S_2 (1^1B_{2g})	86.02	18.88	−61.55	−52.97	−181.20	−159.09

at the D_{4h} and D_{2d} geometries was taken as a sign of non-aromatic behaviour.

It is difficult to tell apart the isotropic shielding pictures observed in the T_1 and S_1 electronic states of COT (Fig. 1, 2 and Fig. S1, S2, ESI†); both of these bear surprisingly close resemblance to the doughnut-shaped region of increased shielding enveloping the carbon framework in the electronic ground state of benzene,[23,24] extended over a ring of eight rather than six carbons atoms. This observation provides compelling visual evidence that the T_1 and S_1 electronic states of COT exhibit levels of aromaticity very similar to that of the electronic ground state of benzene.

The negligible change in the level of aromaticity between the T_1 and S_1 electronic states of COT is one of the differences between the aromaticity characteristics of the low-lying excited states of COT and square cyclobutadiene: In square cyclobutadiene T_1 is noticeably more aromatic than S_1.[24] A second, more important and somewhat unexpected difference is associated with the aromaticity of the second singlet excited state S_2. In square cyclobutadiene S_2 is antiaromatic but less so than S_0.[24] In stark contrast, in the S_2 of COT the interior of the carbon ring is intensively shielded all over (Fig. 1, 2 and Fig. S1, S2, ESI†), in close resemblance to the shielding picture observed in the S_2 state of benzene.[24]

The conclusion that can be drawn from this unexpected finding is that the S_2 electronic state of COT, similarly to the corresponding state of benzene, exhibits a significant level of aromaticity, surpassing that of benzene in its electronic ground state.

Carbon and proton isotropic shieldings and various NICS indices for the S_0, T_1, S_1 and S_2 electronic states of COT, calculated at the same level of theory as the data for the shielding isosurfaces and contour plots, are collected in Table 2. The NICS indices include the original NICS index NICS(0) = $-\sigma_{iso}$(at ring centre),[17] as well as NICS(1) = $-\sigma_{iso}$(at 1 Å above ring centre),[18,19] $NICS(0)_{zz} = -\sigma_{zz}$(at ring centre)[20,21] and $NICS(1)_{zz} = -\sigma_{zz}$(at 1 Å above ring centre).[22] The position at which NICS(1) was evaluated for the non-planar D_{2d} ground state of COT was 1 Å away from the ring centre along the S_4 improper rotation axis. The data for states other than the S_2 electronic state of COT were found to be identical to those reported earlier[10] and have been included in order to facilitate comparison with the rather unexpected magnetic features of this state. According to the NICS(0), NICS(1), $NICS(0)_{zz}$ and $NICS(1)_{zz}$ values for the S_2 electronic state of COT, this state of COT is decidedly more aromatic than the corresponding state of benzene.[24] This conclusion is reinforced by the very significant proton deshielding observed in S_2 COT: the corresponding $\sigma_{iso}(^1H)$ value is more than 8 ppm lower than that in the D_{2d} ground state. Despite the fact that NICS carry much less information than the shielding isosurfaces and contour plots shown in Fig. 1, 2 and Fig. S1, S2 (ESI†), the data included in Table 2 demonstrates that they provide reasonably accurate assessments of the aromaticities of the S_0, T_1, S_1 and S_2 electronic states of COT. Of course, due to their single-point nature, NICS are unable to provide any of the insights into the influence of aromaticity and antiaromaticity on bonding in the S_0, T_1, S_1 and S_2 electronic states of COT that can be analysed and visualised through the respective isotropic shielding isosurfaces and contour plots.

Conclusions

The analysis of the spatial variations in isotropic shielding, $\sigma_{iso}(\mathbf{r})$, at all stationary points of the ground-state PES of COT, including the D_{2d} tub-shaped, D_{4h} bond-alternating and D_{8h} geometries, as well as at the D_{8h} geometries of the lowest triplet and first and second singlet (T_1, S_1 and S_2) electronic excited states reveals both expected and unexpected features of bonding and aromaticity, some of which change dramatically between electronic states.

As expected, the intense antiaromaticity of the electronic ground state at the D_{8h} planar regular octagon geometry experiences rapid decrease on passing, through the lower-energy D_{4h} planar geometry, to the lowest-energy D_{2d} non-planar tub-shaped geometry. Interestingly, even at the D_{2d} geometry, in which the alternating ''single'' and ''double'' carbon–carbon bonds are clearly outlined by the changes in isotropic shielding, ground-state COT retains a hint of antiaromaticity in the form of a small deshielded region surrounding the geometric centre of the molecule.

The features of the first and second singlet excited states of COT revealed by the current magnetic shielding study indicate that Hückel-antiaromatic rings with eight π electrons can be expected to behave differently from square cyclobutadiene in their first and second singlet excited states, with S_1 becoming as aromatic as T_1 and S_2 turning out as strongly aromatic rather than antiaromatic.

The shielding isosurfaces and contour plots suggest that π bonding in the S_2 state of COT (as well as in the S_2 state of benzene[24]) is strengthened, which is associated with increased

shielding within, above and below the ring; this increased shielding creates the perception of a substantially higher level of aromaticity. However, all of this is at the expense of the shielding over the σ framework and the strength of the σ bonds, hence the higher energy of this state. These findings can have important implications for the design of novel photofunctional materials involving flapping molecules[14–16] and suggest that researchers in the area should be advised to examine not only the first singlet excited state of a flapping molecule but also the second singlet excited state—annulation can enhance the σ bond framework, decrease the energy of this state and make it more accessible.

Conflicts of interest

There are no conflicts to declare.

Acknowledgements

We are grateful for support of this work by the University of York.

Notes and references

1 J. I. Wu, I. Fernández, Y. Mo and P. v. R. Schleyer, *J. Chem. Theory Comput.*, 2012, **8**, 1280–1287.
2 M. J. S. Dewar and K. M. Merz, Jr., *J. Phys. Chem.*, 1985, **89**, 4739–4744.
3 D. A. Hrovat and W. T. Borden, *J. Am. Chem. Soc.*, 1992, **114**, 5879–5881.
4 P. G. Wenthold, D. A. Hrovat, W. T. Borden and W. C. Lineberger, *Science*, 1996, **272**, 1456–1459.
5 F.-G. Klärner, *Angew. Chem., Int. Ed.*, 2001, **40**, 3977–3981.
6 J. L. Andrés, O. Castaño, A. Morreale, R. Palmeiro and R. Gomperts, *J. Chem. Phys.*, 1998, **108**, 203–207.
7 A. Schild and B. Paulus, *J. Comput. Chem.*, 2013, **34**, 1393–1397.
8 R. J. F. Berger and A. Viel, *Z. Naturforsch., B: J. Chem. Sci.*, 2020, **75**, 327–339.
9 M. Garavelli, F. Bernardi, A. Cembran, O. Castaño, L. M. Frutos, M. Merchan and M. Olivucci, *J. Am. Chem. Soc.*, 2002, **124**, 13770.
10 P. B. Karadakov, *J. Phys. Chem. A*, 2008, **112**, 12707–12713.
11 N. C. Baird, *J. Am. Chem. Soc.*, 1972, **94**, 4941–4948.
12 V. Gogonea, P. v. R. Schleyer and P. R. Schreiner, *Angew. Chem., Int. Ed.*, 1998, **37**, 1945–1948.
13 F. Feixas, J. Vandenbussche, P. Bultinck, E. Matito and M. Solà, *Phys. Chem. Chem. Phys.*, 2011, **13**, 20690–20703.
14 T. Yamakado, S. Takahashi, K. Watanabe, Y. Matsumoto, A. Osuka and S. Saito, *Angew. Chem., Int. Ed.*, 2018, **57**, 5438–5443.
15 S. Saito, *Flapping Molecules for Photofunctional Materials, in Molecular Technology: Materials Innovation*, ed H. Yamamoto and T. Kato, Wiley-VCH, Weinheim, 2019, vol. 3, pp 17–51.
16 R. Kimura, H. Kuramochi, P. Liu, T. Yamakado, A. Osuka, T. Tahara and S. Saito, *Angew. Chem., Int. Ed.*, 2020, **59**, 16430–16435.
17 P. v. R. Schleyer, C. Maerker, A. Dransfeld, H. Jiao and N. J. R. van Eikema Hommes, *J. Am. Chem. Soc.*, 1996, **118**, 6317–6318.
18 P. v. R. Schleyer, H. Jiao, N. J. R. van Eikema Hommes, V. G. Malkin and O. Malkina, *J. Am. Chem. Soc.*, 1997, **119**, 12669–12670.
19 P. v. R. Schleyer, M. Manoharan, Z. X. Wang, B. Kiran, H. Jiao, R. Puchta and N. J. R. van Eikema Hommes, *Org. Lett.*, 2001, **3**, 2465–2468.
20 I. Cernusak, P. W. Fowler and E. Steiner, *Mol. Phys.*, 2000, **98**, 945–953.
21 E. Steiner, P. W. Fowler and L. W. Jenneskens, *Angew. Chem., Int. Ed.*, 2001, **40**, 362–366.
22 H. Fallah-Bagher-Shaidaei, C. S. Wannere, C. Corminboeuf, R. Puchta and P. v. R. Schleyer, *Org. Lett.*, 2006, **8**, 863–866.
23 P. B. Karadakov and K. E. Horner, *J. Phys. Chem. A*, 2013, **117**, 518–523.
24 P. B. Karadakov, P. Hearnshaw and K. E. Horner, *J. Org. Chem.*, 2015, **81**, 11346–11352.
25 P. B. Karadakov, M. A. H. Al-Yassiri and D. L. Cooper, *Chem. – Eur. J.*, 2018, **24**, 16791–16803.
26 P. B. Karadakov, *Org. Lett.*, 2020, **22**, 8676–8680.
27 P. B. Karadakov, M. Di and D. L. Cooper, *J. Phys. Chem. A*, 2020, **124**, 9611–9616.
28 C. Foroutan-Nejad, S. Shahbazian, F. Feixas, P. Rashidi-Ranjbar and M. Solà, *J. Comput. Chem.*, 2011, **32**, 2422–2431.
29 C. Foroutan-Nejad, *Theor. Chem. Acc.*, 2015, **134**(8), 1–9.
30 S. Fias, P. W. Fowler, J. L. Delgado, U. Hahn and P. Bultinck, *Chem. – Eur. J.*, 2008, **14**, 3093–3099.
31 S. Van Damme, G. Acke, R. W. A. Havenith and P. Bultinck, *Phys. Chem. Chem. Phys.*, 2016, **18**, 11746–11755.
32 K. Aidas, C. Angeli, K. L. Bak, V. Bakken, R. Bast, L. Boman, O. Christiansen, R. Cimiraglia, S. Coriani, P. Dahle, E. K. Dalskov, U. Ekström, T. Enevoldsen, J. J. Eriksen, P. Ettenhuber, B. Fernández, L. Ferrighi, H. Fliegl, L. Frediani, K. Hald, A. Halkier, C. Hättig, H. Heiberg, T. Helgaker, A. C. Hennum, H. Hettema, R. Hjertenæs, S. Høst, I.-M. Høyvik, M. F. Iozzi, B. Jansík, H. J. Aa. Jensen, D. Jonsson, P. Jørgensen, J. Kauczor, S. Kirpekar, T. Kjærgaard, W. Klopper, S. Knecht, R. Kobayashi, H. Koch, J. Kongsted, A. Krapp, K. Kristensen, A. Ligabue, O. B. Lutnæs, J. I. Melo, K. V. Mikkelsen, R. H. Myhre, C. Neiss, C. B. Nielsen, P. Norman, J. Olsen, J. M. H. Olsen, A. Osted, M. J. Packer, F. Pawlowski, T. B. Pedersen, P. F. Provasi, S. Reine, Z. Rinkevicius, T. A. Ruden, K. Ruud, V. V. Rybkin, P. Sałek, C. C. M. Samson, A. Sánchez de Merás, T. Saue, S. P. A. Sauer, B. Schimmelpfennig, K. Sneskov, A. H. Steindal, K. O. Sylvester-Hvid, P. R. Taylor, A. M. Teale, E. I. Tellgren, D. P. Tew, A. J. Thorvaldsen, L. Thøgersen, O. Vahtras, M. A. Watson, D. J. D. Wilson, M. Ziolkowski and H. Ågren, *Wiley Interdiscip. Rev.: Comput. Mol. Sci.*, 2014, **4**, 269–284, Dalton, a molecular electronic structure program, Release Dalton2018.1, 2019, see http://daltonprogram.org.

33 M. J. Frisch, G. W. Trucks, H. B. Schlegel, G. E. Scuseria, M. A. Robb, J. R. Cheeseman, G. Scalmani, V. Barone, G. A. Petersson, H. Nakatsuji, X. Li, M. Caricato, A. V. Marenich, J. Bloino, B. G. Janesko, R. Gomperts, B. Mennucci, H. P. Hratchian, J. V. Ortiz, A. F. Izmaylov, J. L. Sonnenberg, D. Williams-Young, F. Ding, F. Lipparini, F. Egidi, J. Goings, B. Peng, A. Petrone, T. Henderson, D. Ranasinghe, V. G. Zakrzewski, J. Gao, N. Rega, G. Zheng, W. Liang, M. Hada, M. Ehara, K. Toyota, R. Fukuda, J. Hasegawa, M. Ishida, T. Nakajima, Y. Honda, O. Kitao, H. Nakai, T. Vreven, K. Throssell, J. A. Montgomery, Jr., J. E. Peralta, F. Ogliaro, M. J. Bearpark, J. J. Heyd, E. N. Brothers, K. N. Kudin, V. N. Staroverov, T. A. Keith, R. Kobayashi, J. Normand, K. Raghavachari, A. P. Rendell, J. C. Burant, S. S. Iyengar, J. Tomasi, M. Cossi, J. M. Millam, M. Klene, C. Adamo, R. Cammi, J. W. Ochterski, R. L. Martin, K. Morokuma, O. Farkas, J. B. Foresman and D. J. Fox, *Gaussian 16, Revision A.03*, Gaussian, Inc., Wallingford CT, 2016.
34 K. Ruud, T. Helgaker, R. Kobayashi, P. Jørgensen, K. L. Bak and H. J. A. Jensen, *J. Chem. Phys.*, 1994, **100**, 8178–8185.
35 K. Ruud, T. Helgaker, K. L. Bak, P. Jørgensen and J. Olsen, *Chem. Phys.*, 1995, **195**, 157–169.
36 P. B. Karadakov, *J. Phys. Chem. A*, 2008, **112**, 7303–7309.
37 P. W. Fowler, E. Steiner and L. W. Jenneskens, *Chem. Phys. Lett.*, 2003, **371**, 719–723.
38 Z. Rinkevicius, J. Vaara, L. Telyatnyk and O. Vahtras, *J. Chem. Phys.*, 2003, **118**, 2550–2561.
39 J. Vaara, *Phys. Chem. Chem. Phys.*, 2007, **9**, 5399–5418.
40 See https://gaussian.com/cubegen/(checked on 24 September 2021).
41 P. B. Karadakov and K. E. Horner, *J. Chem. Theory Comput.*, 2016, **12**, 558–563.
42 K. E. Horner and P. B. Karadakov, *J. Org. Chem.*, 2013, **78**, 8037–8043.
43 K. E. Horner and P. B. Karadakov, *J. Org. Chem.*, 2015, **80**, 7150–7157.
44 P. B. Karadakov, J. Gerratt, D. L. Cooper and M. Raimondi, *J. Phys. Chem.*, 1995, **99**, 10186–10195.

